Cell, Vol. 107, 373–386, November 2, 2001, Copyright ©2001 by Cell Press

Structure of the 80S Ribosome from *Saccharomyces cerevisiae*— tRNA-Ribosome and Subunit-Subunit Interactions

Christian M.T. Spahn,[1,2,9] Roland Beckmann,[4,5,9] Narayanan Eswar,[6] Pawel A. Penczek,[7] Andrej Sali,[6] Günter Blobel,[4] and Joachim Frank[1,2,3,8]

[1]Howard Hughes Medical Institute,
Health Research Inc.
[2]Wadsworth Center
Empire State Plaza
Albany, New York 12201
[3]Department of Biomedical Science
State University of New York at Albany
Albany, New York 12222
[4]Laboratory of Cell Biology
Howard Hughes Medical Institute
The Rockefeller University
1230 York Avenue
New York, New York 10021
[5]Institut für Biochemie der Charité
Humboldt Universität zu Berlin
Monbijoustr. 2, 10117
Berlin
Germany
[6]Laboratory of Molecular Biophysics
Pels Family Center for Biochemistry and Structural Biology
The Rockefeller University
New York, New York
[7]University of Texas—Houston Medical School
6431 Fannin
Houston, Texas 77030

Summary

A cryo-EM reconstruction of the translating yeast 80S ribosome was analyzed. Computationally separated rRNA and protein densities were used for docking of appropriately modified rRNA models and homology models of yeast ribosomal proteins. The core of the ribosome shows a remarkable degree of conservation. However, some significant differences in functionally important regions and dramatic changes in the periphery due to expansion segments and additional ribosomal proteins are evident. As in the bacterial ribosome, bridges between the subunits are mainly formed by RNA contacts. Four new bridges are present at the periphery. The position of the P site tRNA coincides precisely with its prokaryotic counterpart, with mainly rRNA contributing to its molecular environment. This analysis presents an exhaustive inventory of an eukaryotic ribosome at the molecular level.

Introduction

The translation of the genetic message is carried out by ribosomes, large macromolecular machines that consist of ribosomal RNA (rRNA) and 50–80 ribosomal proteins (Green and Noller, 1997). Recently, the structures of the small 30S subunit from the thermophile bacterium *Thermus thermophilus* (Schlünzen et al., 2000; Wimberly et al., 2000) and the large 50S subunit from the halophile archaebacterium *Haloarcula marismortui* (Ban et al., 2000) were solved by X-ray crystallography. These landmark structures indicate that ribosomes are RNA-based machines, in agreement with biochemical evidence (Green and Noller, 1997; Noller, 1991). The 23S rRNA of the large subunit is responsible for the catalytic activity of the ribosome, the peptidyl transferase activity (Nissen et al., 2000), while the 16S rRNA of the small subunit is used almost exclusively for the decoding process, the selection of the cognate tRNA (Carter et al., 2000). The atomic models of the ribosomal subunits, together with structural investigations of functional ribosomal complexes by X-ray crystallography (Cate et al., 1999; Yusupov et al., 2001; Carter et al., 2001; Ogle et al., 2001; Pioletti et al., 2001) and 3D cryo-EM (Agrawal and Frank, 1999; Agrawal et al., 2000; Frank and Agrawal, 2000; Gabashvili et al., 2000; Stark et al., 1997a, 1997b, 2000), will eventually lead to an understanding of the structure and dynamics of protein biosynthesis.

Most information about the ribosome has been obtained in prokaryotic systems. In contrast, our knowledge about eukaryotic ribosomes is sparse. Because of the evolutionary conservation of rRNA and ribosomal proteins, it can be anticipated that the ribosomal subunits share a similar spatial arrangement and that the fundamental mechanism of protein biosynthesis is the same. However, the actual degree of similarity of the whole ribosomes is not known, and significant differences are known to exist. Due to insertion elements in the rRNA molecules (Gerbi, 1996) and the presence of 20 to 30 additional proteins (Wittmann-Liebold, 1986; Wool et al., 1990; Planta and Mager, 1998), eukaryotic ribosomes are larger than their prokaryotic counterparts (Figure 1). There are functional differences, especially in the mechanism of initiation, which is far more complex in eukaryotes (Sachs et al., 1997). There are also differences in the elongation phase; e.g., yeast has a third elongation factor, EF3 (Triana-Alonso et al., 1995), and several antibiotics are specific for one class of ribosomes or the other (Spahn and Prescott, 1996). These and other differences in function are likely to be reflected by differences in structure.

Furthermore, the ribosome has to play a role in other biological processes in the cell, such as protein transport (Beckmann et al., 1997; Menetret et al., 2001; Beckmann et al., 2001) and protein folding (Hardesty et al., 2000), and is subjected in eukaryotes to a transport process through the nuclear pore complex (Ho et al., 2000). Binding and recognition events in these processes do not necessarily take place at those ribosomal sites that are highly conserved among bacterial and eukaryotic ribosomes. Therefore, structural understanding of protein biosynthesis and related processes in eukaryotes will depend on the availability of structural information about the 80S ribosome.

We present here a molecular analysis of the translat-

[8]Correspondence: joachim@wadsworth.org
[9]These authors contributed equally to this work.

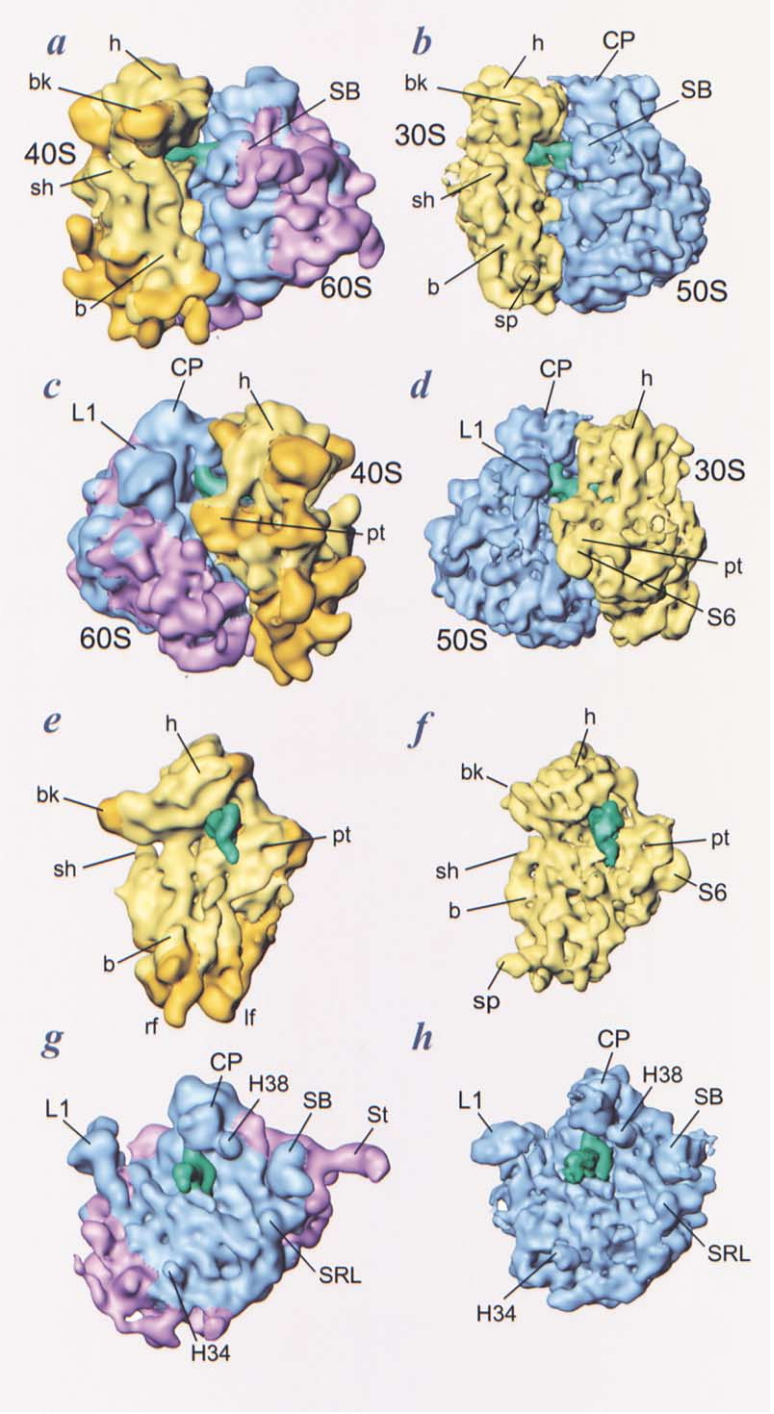

Figure 1. Comparison of the 80S Ribosome from *S. cerevisiae* with the *E. coli* 70S Ribosome

The cryo-EM map of the yeast 80S ribosome (a, c, e, and g) is shown together with the cryo-EM map of the *E. coli* 70S ribosome (b, d, f, and h; Gabashvili et al., 2000). The ribosomes are shown from the L7/L12 side (a and b) and the L1 side (c and d). The computationally isolated small subunits (e and f) and large subunits (g and h) are shown from the interface sides. The small subunits are in yellow, the large subunits in blue, and the P site-bound tRNA in green. Additional parts of the eukaryotic 80S ribosome that are due to expansion segments in the rRNAs (Figure 2) and nonhomologous proteins are shown in gold (40S subunit) and purple (60S subunit). Landmarks for the 40S subunit: b, body; bk, beak; h, head; lf, left foot; rf, right foot; pt, platform; sh, shoulder; sp, spur. Landmarks for the 60S subunit: CP, central protuberance; L1, L1 protuberance; SB, stalk base; St, L7/L12 stalk; H34, helix 34; H38, helix 38; SRL, sarcin-ricin loop.

ing 80S ribosome from yeast by combining a cryo-EM map at approximately 15 Å resolution (Figure 1, see Beckmann et al., 2001) with molecular rRNA and protein models. This analysis reveals the positions of all major rRNA expansion elements and of additional proteins. The model of the 80S ribosome derived describes the intersubunit bridges and the contacts between the 80S ribosome and the P site-bound peptidyl-tRNA at the molecular level. In the accompanying paper, this model is used to derive molecular information about the interaction of the 80S ribosome with the protein-conducting channel Sec61 (Beckmann et al., 2001 [this issue of *Cell*]).

Results and Discussion

Docking of Atomic Models into the Cryo-EM Map

In the absence of an atomic resolution map of a macromolecular complex, docking of atomic models of its components into a lower-resolution cryo-EM map is a

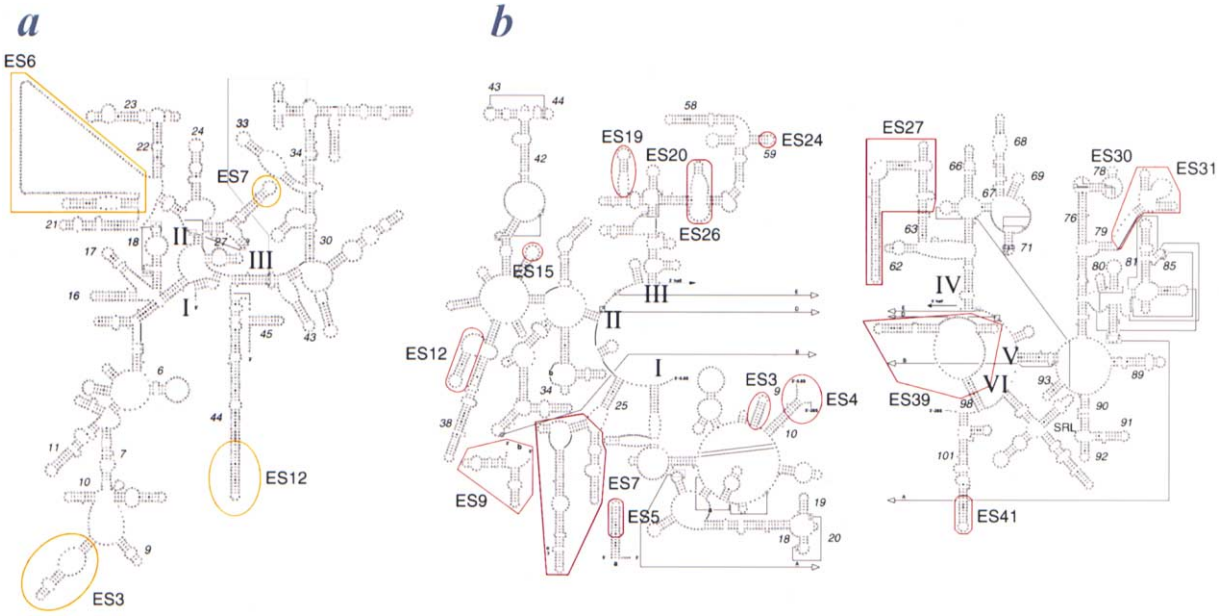

Figure 2. rRNA Secondary Structure Diagrams

Secondary structure diagrams of the 18S rRNA (a) and the 5.8/25S rRNA (b) of *S. cerevisiae* (http://www.rna.icmb.utexas.edu). Expansion segments in the rRNAs are indicated, using the nomenclature of Gerbi (1996).

powerful tool to obtain molecular level information about at least part of the macromolecular assembly. It is estimated that atomic models of known substructures can be positioned in a cryo-EM map with accuracy exceeding the resolution of the map several-fold (Rossmann, 2000).

To facilitate the docking, the map of the 80S ribosome was computationally separated (Spahn et al., 2000) into rRNA and protein maps (Figures 3–5). rRNA models of the recently solved crystal structures of the 30S subunit from *T. thermophilus* (Wimberly et al., 2000) and the 50S subunit from *H. marismortui* (Ban et al., 2000) were fitted into the resulting maps for the small subunit (SSU) rRNA (Figures 3c–3f) and large subunit (LSU) rRNA of yeast (Figure 5), respectively. Where necessary, the X-ray models were modified by moving nonfitting parts (e.g., helices) as rigid bodies relative to the rest of the model. Homology models were calculated for those yeast ribosomal proteins that were found to be related to a bacterial or an archaebacterial protein of known 3D structure. In total, homology models were obtained for 43 yeast ribosomal proteins (15 for the 40S subunit [Figures 3a and 3b], 28 for the 60S subunit [Figure 4]) and positioned in the protein map of the 80S ribosome. In calculating the homology models, it was advantageous that the X-ray structure of the 50S subunit was from an archaebacterial species, since the protein composition of eukaryotic ribosomes is more closely related to archaebacterial ribosomes than to bacterial ones.

Accuracy of the RNA-protein separation method is not absolute; e.g., flexible RNA can be assigned to the protein map, and a small protein cluster to the rRNA map. However, the overall agreement of the separated maps with the atomic models is very good. There is generally excellent agreement between the shape of the protein densities and the homology models, showing that the observed sequence similarities are indeed reflected in conserved tertiary structures (Figures 3 and 4). Prediction of extended protein tails (Ban et al., 2000; Schlünzen et al., 2000; Wimberly et al., 2000) or smaller parts of a protein that intimately interact with rRNA is, of course, beyond the resolution limit of the current cryo-EM map of the yeast 80S ribosome. However, in the case of evolutionary conservation of such protein segments, their positions within the 80S ribosome can be inferred from the atomic structures of the prokaryotic ribosomal subunits, as can the positions of the three proteins (rpS13, rpL19, and rpL42) whose density was assigned to the RNA partition.

The 40S Subunit versus the 30S Subunit

The 40S ribosomal subunit shows the classical division into head, body, and platform (Verschoor et al., 1998; Dube et al., 1998). However, it is not easy to align the overall shape of the 40S subunit from yeast with the bacterial 30S subunit. Due to extra density in the 40S subunit and a change in orientation of some elements, the 40S subunit is longer than its bacterial counterpart and shows a strong subdivision at the bottom part of the body into a "left foot" and a "right foot" (Figure 1). Extra density is mainly present (1) at the bottom of the 40S subunit, responsible for the increase in length of the subunit, (2) below the platform, forming the "left foot" and the "back lobe" of the 40S subunit, (3) at the "beak," and (4) at the solvent side of the head, building the "head lobe."

The 40S ribosomal subunit of *S. cerevisiae* is composed of the 1798 nucleotide (nt)-long 18S rRNA and 32 ribosomal proteins. The 18S rRNA is 256 nt longer than the 16S rRNA of *E. coli*, and the yeast 40S subunit contains 11 more proteins than the 30S subunit from *E. coli*. Consequently, both insertion elements in the 18S rRNA (Figure 2a) and additional ribosomal proteins (Sup-

plemental Table S1) are responsible for the extra mass of the small subunit in eukaryotes.

The Structure of the 18S rRNA

The X-ray model of the 16S rRNA is in good agreement with the map of the 18S rRNA in the region that corresponds to the common core of the SSU rRNA, showing that the phylogenetic conservation of secondary structure is indeed reflected in the conservation of the tertiary structure. However, some differences due to conformational changes are apparent. An unexpected difference is in the conformation of the 18S rRNA helices that make up the shoulder of the 40S subunit (i.e., helices 16 and 17; Figure 3). In bacterial 30S subunits, helix 16 is folded toward helix 18 (the 530 pseudoknot structure), and helix 17 runs parallel to the long axis of the subunit toward the bottom of the body domain (Wimberly et al., 2000; Schlünzen et al., 2000; Spahn et al., 2000). In the yeast 40S subunit, helix 16 is rotated toward the back side of the subunit where it sticks out into the solvent (Figure 3). Helix 17 is shorter in yeast, containing more irregular base pairs. It appears to make a sharp turn below the position of protein rpS9 (S4p; Figure 3b) and folds toward the apical loop of helix 21 (Figure 3d). Helix 16 in a mammalian 40S subunit has the same conformation as in the yeast 40S; it becomes broadly fused with the head domain upon binding of the HCV IRES (Spahn et al., 2001). Therefore, the difference in the shoulder region between bacteria and eukaryotes might be important for the distinct mechanisms of translation initiation.

Another difference between prokaryotic and eukaryotic 40S subunits is in the position and shape of the beak. The corresponding rRNA element, helix 33, is slightly longer in yeast than helix 33 of 16S rRNA, but it does not contain helix 33a, so that the overall rRNA element is shorter (Figure 2a). The curvature of the beak is less pronounced in yeast and its length is increased (Figures 1e and 1f) due to the presence of an additional protein (Figure 3, see below). Finally, there are differences between yeast 18S rRNA and *T. thermophilus* 16S rRNA in the position of the lower part of the body. In yeast it is located more toward the side of the shoulder, a difference which also affects the lower part of helix 44. A movement of components of the lower body in this direction has also been observed when the structure of the vacant *T. thermophilus* 30S subunit was compared with the 50S-bound 30S subunit of *E. coli* (Gabashvili et al., 2000). Therefore, this conformational change might be at least in part due to subunit association.

A straightforward localization of an insertion element is possible wherever unaccounted density is present in the 18S rRNA map and the comparison of the secondary structure diagrams reveals an insertion (Figures 3e and 3f). Helix 44 is clearly resolved, and its extension (ES12) builds the "right foot" of the 40S subunit (cf. Dube et al., 1998). ES6, the helix 21 insertion, emerges at the solvent side of the platform, appearing to branch into two irregular helices (Figure 3f). The smaller of these helices builds one of the "back lobes" and runs toward the shoulder, parallel to helix 21. The larger branch runs toward the bottom, constituting the "left foot" (Figures 3e and 3f). At its lower end, it appears to interact with expansion segment ES3. This structure creates a network of interactions connecting the platform of the 40S subunit with the lower part of the body, a feature that is specific to eukaryotic ribosomes.

The Distribution of Proteins in the 40S Subunit

Fifteen of the SSU proteins of yeast have homologous proteins in bacteria (Supplemental Table S1), while seventeen have no homologous counterparts. Density in the 40S protein map that is not accounted for by homology models predicts the locations of these proteins or of additional domains in the homologous proteins (Figure 3). There are eight regions with additional protein density, most of which are present at the solvent side of the 40S subunit (Figure 3b). Two such clusters of protein density are in the head of the 40S subunit, where they build the headlobe, located above protein rpS0 (S2p), and part of the beak, replacing helix 33a of the 16S rRNA (Figure 3). The protein density at the top of the platform surrounding rpS14 (S11p) is enlarged, leading to a stronger contact with rpS5 (S7p) (Figure 3). This head-platform interaction defines part of the mRNA exit channel. Also, the region around protein rpS0 (S2p) is enlarged, with additional protein density being present at the branch site of the helix 21 insertion (ES6) in 18S rRNA. Another large cluster of protein density is located below helix 21 of 18S rRNA where it "replaces" the bacterial protein S16 (Figure 3b). The presence of this protein cluster might be responsible, to some extent, for the difference in the path of helix 17 of the SSU rRNA (Figures 3c and 3f, see above). Finally, two protein clusters are at the 60S side of the 40S subunit at the bottom of the "left" and "right foot" (Figure 3a). The protein cluster at the "left foot" is at a similar position as the bacterial S20p protein, which has no homologous protein in eukaryotes. A more detailed analysis is unfortunately not possible at this time, because data on the quaternary structure of eukaryotic ribosomes by IEM, cross-linking, or footprinting experiments are scarce.

Four bacterial SSU proteins do not have detectably homologous eukaryotic proteins, but two of these proteins, S16p and S20p, might have analogous counterparts (see above). Interestingly, however, there is no protein density corresponding to proteins S6p and S18p, leaving the 18S rRNA (the junction between helices 22 and 23; Figure 2a) accessible at the solvent side of the platform (Figures 1 and 3). This difference might have functional implications, since the IRES element of HCV binds the 40S subunit in this region (Spahn et al., 2001).

The 60S Subunit versus the 50S Subunit

The 60S ribosomal subunit of *S. cerevisiae* is built from 25S rRNA (3392 nt), 5.8 S rRNA (158 nt), 5S rRNA (121 nt), and 45 ribosomal proteins. Since the 5.8S rRNA is homologous to the 5′-region of the 23S rRNA, the LSU rRNA (Figure 2b) in yeast is 646 nt longer than the bacterial 23S rRNA from *E. coli* (2904) and 505 nt longer than the archaebacterial 23S rRNA from *H. marismortui* (3045 nt). The yeast 60S subunit has 12 proteins more than the *E. coli* 50S subunit (33 different proteins) and 14 proteins more than the *H. marismortui* 50S subunit (31 proteins).

As in the case of the 40S subunit, the atomic model of the *H. marismortui* 23S rRNA (Ban et al., 2000) could

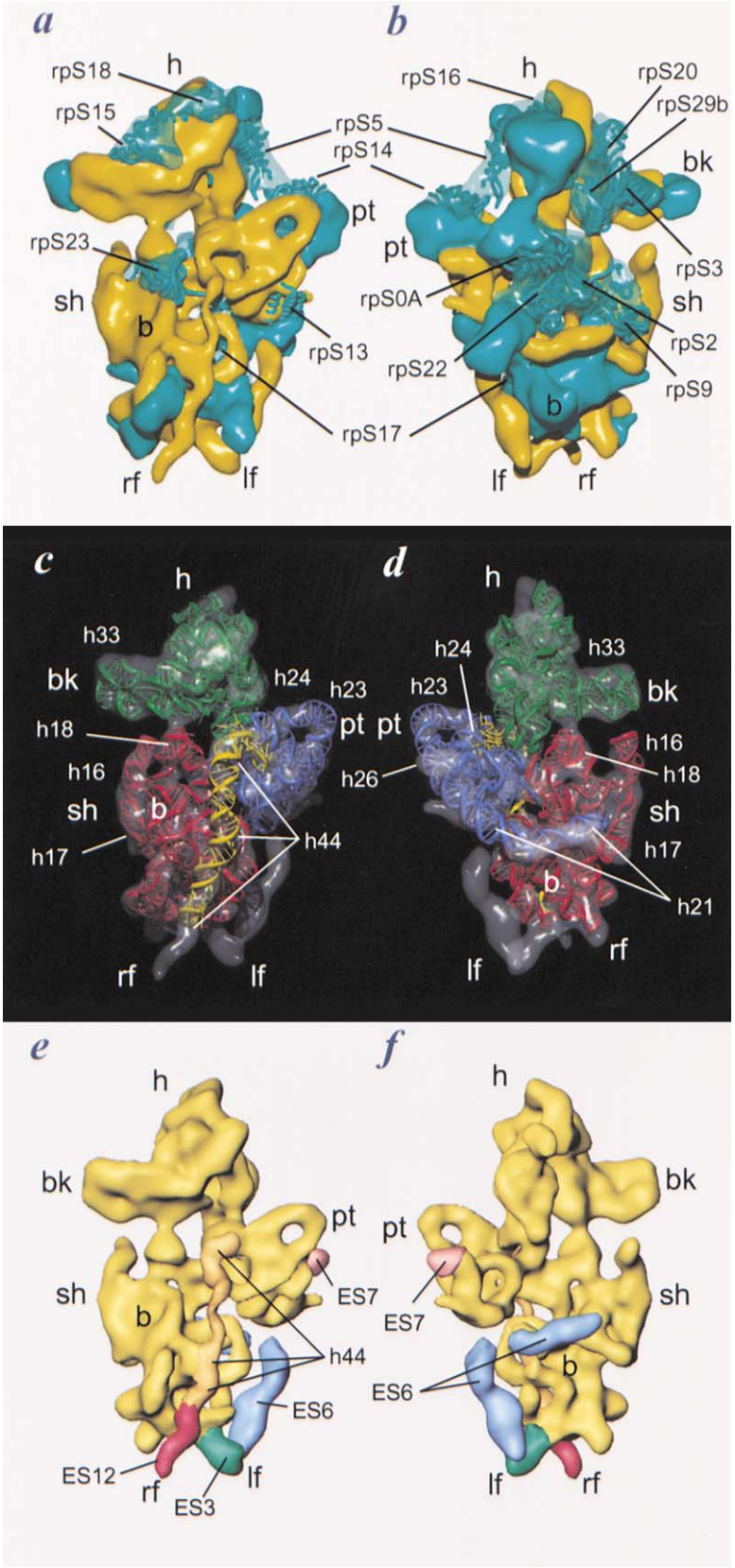

Figure 3. RNA versus Protein Separation for the 40S Subunit

The 40S subunit is shown from the intersubunit side (a, c, and e) and the solvent side (b, d, and f).

(a and b) The RNA partition is in yellow at high contour level; the protein partition is in turquoise. Wherever homology models could be docked into the map, the protein partition is shown with transparency. Therefore, solid parts of the protein partition predict the position of additional proteins without homologous counterparts in prokaryotes. The fitted homologous proteins are shown as ribbon models (Carson, 1991) and are designated with their name.

(c and d) The RNA map is shown transparently superposed on the ribbons model for the common conserved core of the 18S rRNA. The domains of the ribbons model for the SSU rRNA are color coded: domain I, red; domain II, blue; domain III major, green; domain III minor, yellow.

(e and f) The common core of the 18S rRNA is shown in yellow with helix 44 and the expansion segments (defined in Figure 2a) highlighted in different colors. Several helices of the 18S rRNA are annotated with their numbers. Landmarks of the 40S subunit are as in Figure 1.

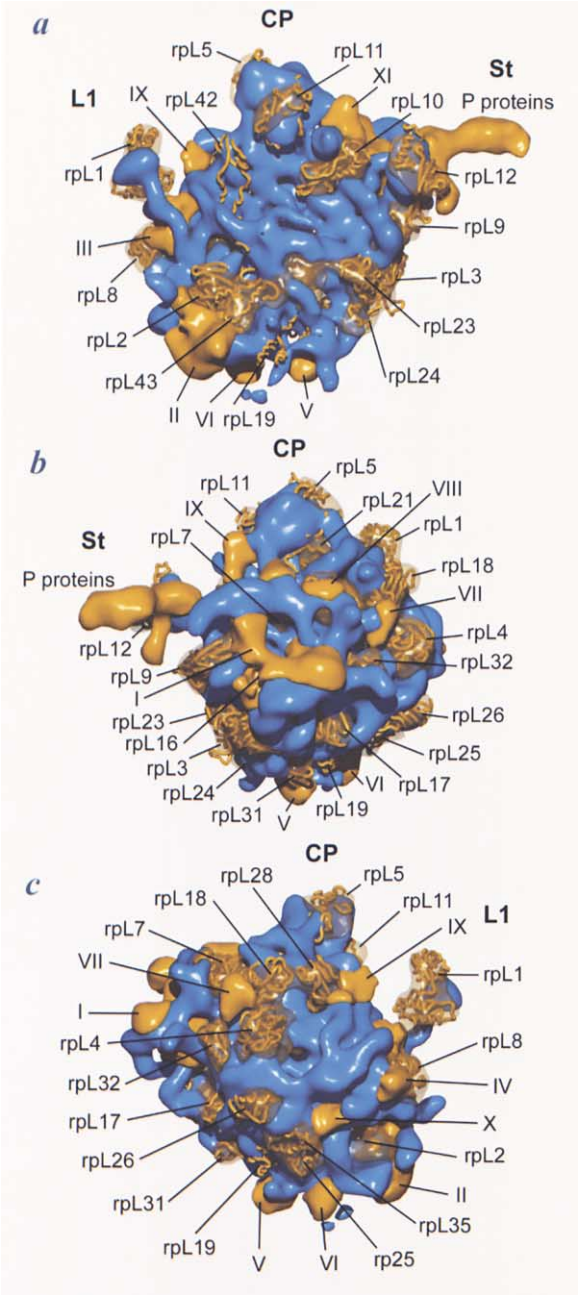

Figure 4. RNA and Protein Separation for the 60S Subunit and Docking of Homology Models for the Proteins

The 60S subunit is shown from the intersubunit side, in the classical crown view (a), from the bottom of the L7/L12 side (b), and from the bottom of the L1 side (c). The RNA partition is shown in blue at a high contour level; the protein partition is in orange. Wherever homology models could be docked into the map, the protein partition is shown transparently. Therefore, solid parts of the protein partition predict the position of additional proteins with no homologous counterpart in prokaryotes. These clusters of density are labeled with a Roman numeral, and the neighboring components are summarized in Supplemental Table S3. The fitted homologous proteins are shown as ribbon models and are designated with their name.

be fitted well into the RNA map of the 60S subunit, again indicating a conserved tertiary core of the 25S rRNA (Figure 5). The X-ray structure of the 50S subunit is disordered in the L1 and L11 regions, so the 25S rRNA model (Figure 5) was supplemented with the L1 region of domain IV of 23S rRNA from *T. thermophilus* (Yusupov et al., 2001) and L11 binding RNA from *T. maritima* (Wimberly et al., 1999), respectively. However, the position of some elements had to be readjusted to achieve a satisfying agreement with the EM density. The underlying conformational changes concern (i) domain VI of 25S rRNA, (ii) helices 7, 18, 19, 20, and 24 of domain I around the exit site of the nascent peptide, (iii) helix 25, (iv) the sarcin-ricin loop (SRL) with helices 89 and 91, (v) helix 42 that leads to the stalk base, and (vi) 5S rRNA. These conformational changes might be species-specific as in the case of helix 25 (see below), but, since these changes are relatively small and located in functionally important regions, they might be caused by subunit association or the active functional state of the 80S ribosome. Compared to the recent X-ray structure of the *T. thermophilus* 70S ribosome (Yusupov et al., 2001), large differences can be seen at the L1- and L11-bearing protuberances. The L11-bearing helices 43 and 44 are shifted by approximately 15 Å toward the central protuberance in *T. thermophilus*; the L1-bearing helix 78, by even more than 30 Å. Movements of both protuberances by a similar magnitude have been observed previously in the yeast ribosome in response to EF2 binding (Gomez-Lorenzo et al., 2000). Both protuberances are apparently highly dynamic, in line with their emerging roles in facilitating the entering and exiting of the tRNAs.

A pronounced species-related conformational change can be observed in the LSU rRNA when the 80S ribosome from *S. cerevisiae* is compared to the 70S ribosome from *E. coli* (Gabashvili et al., 2000), which also carries a tRNA in the P site. Helix 58 of domain III of the LSU rRNA occupies the same position in the archaebacterium *H. marismortui* (Ban et al., 2000) and in yeast, and is located at the bottom of the subunit below the L1 protuberance (Figure 5a). In contrast, in the *E. coli* 70S ribosome and also in the recent X-ray structure of the *T. thermophilus* 70S ribosome (Yusupov et al., 2001), this helix is folded upwards such that it runs along protein L2 toward the apical loops of helices 10 and 79 of 23S rRNA. The apical loop of helix 58 is shifted by more than 50 Å in the bacterial 70S ribosome when compared to its position in the archaebacterial 50S subunit or the eukaryotic 80S ribosome.

Expansion Segments in the 5.8S/25S rRNA

The yeast LSU rRNA contains several expansion segments (Gerbi, 1996; Gutell et al., 2001) that were identified as extra density in the separated RNA map, unaccounted for by the X-ray model of the *H. marismortui* 23S rRNA. Expansion segments are distributed over the whole 5.8S/25S rRNA and are present in all 6 domains (Figure 2b). The expansion segments are located at the surface, roughly at two opposite sides of the 60S subunit (Figure 5). One region is behind the central protuberance and the stalk region, when looking at the 60S subunit in the crown view; the other region extends from the bottom of the 60S to the base of the L1 protuberance. The expansion segments are not mere solvent-exposed protuberances, but are frequently involved in tertiary and quaternary contacts, providing additional interdomain interactions. Two expansion segments even form

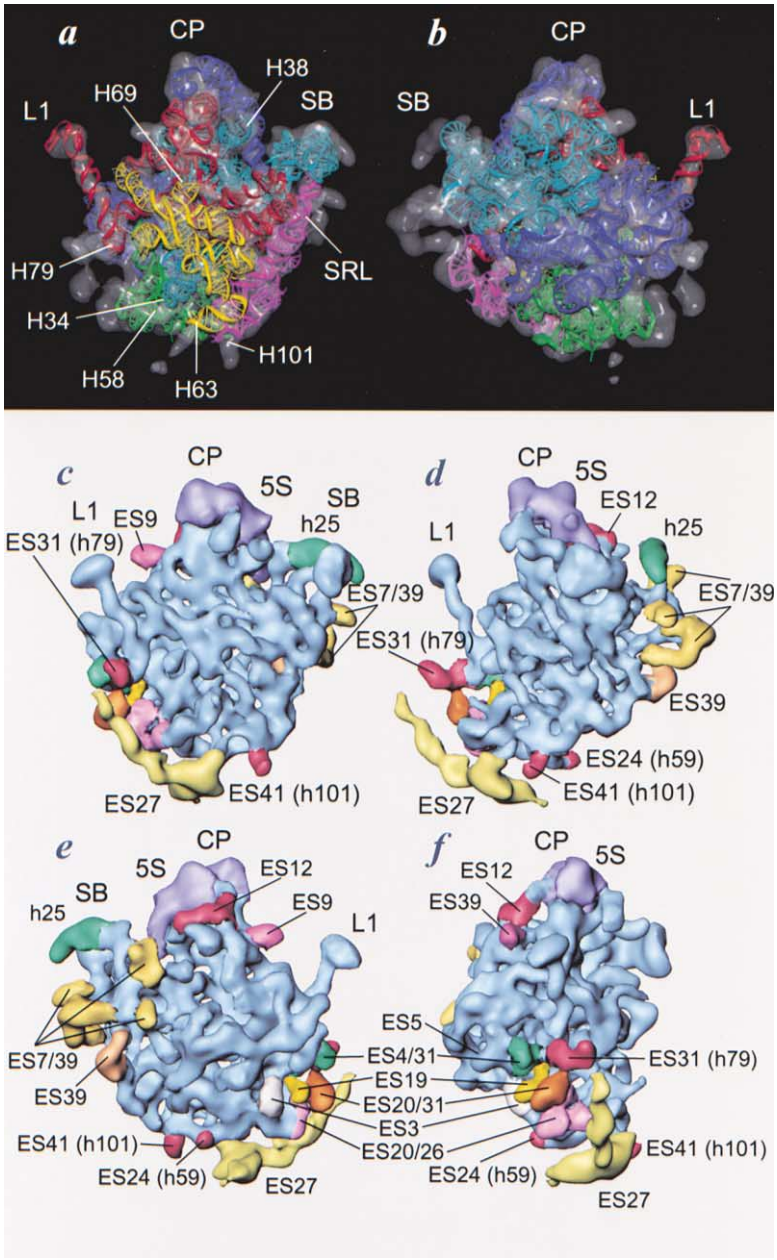

Figure 5. High-Threshold Rendering of the RNA Partition of the 60S Subunit

(a and b) The RNA map is shown transparently superposed with the ribbons model for the common conserved core of the 5.8S/25S and 5S rRNAs. The domains of the ribbons model for the LSU rRNA are color coded: domain I, blue; domain II, cyan; domain III, green; domain IV, yellow; domain V, red; domain VI, magenta; 5S rRNA, blue.

(c–f) The common core of the LSU rRNA is shown in blue, with the expansion segments (defined in Figure 2b) highlighted in different colors. The RNA map is shown from the intersubunit side (a and c), the solvent side (b and e), the L7/L12 side (d), and the L1 side (f). Several helices of the LSU rRNA are annotated with their number. Landmarks are as in Figure 1.

additional bridges with the 40S subunit (Figure 6, see below).

Expansion segments in 25S rRNA domains II and VI (Figure 2b) are responsible for the additional RNA density behind the stalk region (Figure 5). Domain II of 25S rRNA contains a major expansion segment in helix 25, ES7. However, it cannot be completely resolved, since it is broadly fused with another major expansion segment, ES39, and it has a fragmented appearance, apparently because some part of the RNA was assigned to the protein partition in the density separation, indicating flexibility (see Spahn et al., 2000). ES39 is an addition to helix 98 in domain VI (Figure 2b). Helix 98 is missing in *H. marismortui* but has been identified by genetic tagging in *E. coli* ribosomes (Spahn et al., 1999). The beginning of ES39 in 25S rRNA is resolved (Figure 5) before it becomes fused with ES7, and its orientation is similar to that of helix 98 in *E. coli*.

Two smaller insertions into domain II of 25S rRNA, ES9 and ES12, are located at the back of the central protuberance (Figure 5e). ES12, an insertion into helix 38, appears to be of mechanistic interest because of the prominent role of helix 38: it is involved in the formation of a bridge with the 40S subunit and in forming a contact with the elbow of the A site-bound tRNA (A site finger). ES12 runs at the back of the central protuberance toward the L1 side of the ribosome (Figures 5e and 5f). It might act as a strut that could, together with 5S rRNA, be involved in the coupling of conformational changes of ribosomal components that interact with the elbow regions of A and P site-bound tRNAs. At its apical loop, it makes contact with a eukaryote-specific sequence of the 5S rRNA binding protein rpL5 (L18p). rpL5 (L18p) and rpL11 (L5p) interact directly with each other as well as indirectly via 5S rRNA. rpL11 (L5p), similarly to helix 38 in the A site, interacts with the elbow of the

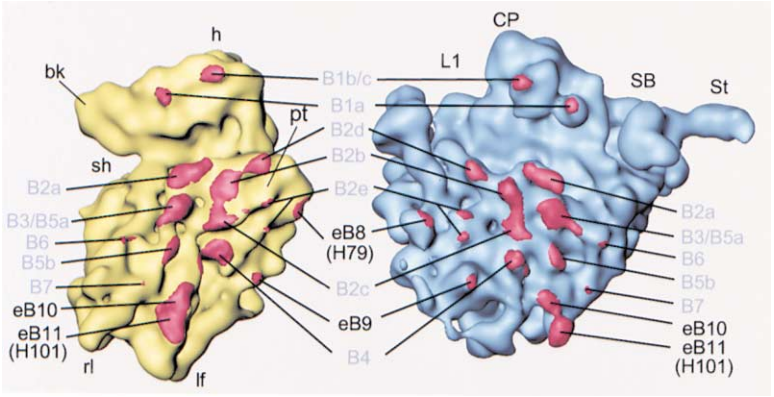

Figure 6. Position of the Intersubunit Bridges

The 40S subunit in yellow (a) and the 60S subunit in blue (b) are shown from their intersubunit sides. The intersubunit bridges are shown in red and are annotated with their numbers. Bridges also observed in prokaryotic ribosomes are numbered B1–B7. Additional intersubunit connections in the yeast ribosome are named eB8–eB11 (see also Table 1).

P site-bound tRNA and is also involved in the formation of a bridge with the 40S subunit (Figures 4–6).

Insertions into domains I, II, and V of 5.8S/25S rRNA appear to form a new network of strands below the L1 stalk (Figure 5). This additional cluster of density is formed by ES4, ES5, ES19, ES20, ES26, and ES31. Interestingly, due to the additional rRNA elements, helix 79 of 25S rRNA undergoes tertiary contacts via ES31 with domains I and III. Helix 79, in turn, is stacked on the protein L1-bearing helix 76, an arrangement which might have implications for the large movement of the L1 stalk observed in the yeast ribosome (Gomez-Lorenzo et al., 2000). Furthermore, ES31 is involved in the formation of an intersubunit bridge (Figure 6, see below). Adjacent to this region, the cluster of expansion segments around ES31 forms another connection between domains I and III of 5.8S/25S rRNA. Helix 9, which is absent in the *H. marismortui* 23S rRNA, appears to interact with helix 54 (Figure 5). An equivalent connection can be observed in the cryo-EM map of the *E. coli* 70S ribosome.

The third major insertion into yeast 25S rRNA, ES27 in helix 63, is located at the L1 side, toward the bottom of the 60S subunit (Figure 5). Helix 63 runs at the bottom of the intersubunit face of the 60S subunit from the L7 side (L7/L12 is replaced in eukaryotes by the acidic P proteins) to the L1 side. This feature is consistent with the location of helix 63 in *E. coli* (Spahn et al., 1999), which is larger than its *H. marismortui* counterpart. At the position of the apical loop of helix 63 in *E. coli*, the additional RNA density emerges from the 25S rRNA (Figure 5). In agreement with the predicted secondary structure, ES27 consists of a more convoluted RNA structure, from which a long rod emerges that runs up at the L1 side of the 60S subunit (Figure 5). This rod has clear helical features, and a part of it was also named "yeast spine" in a lower-resolution cryo-EM structure of the yeast 80S ribosome (Morgan et al., 2000). In our present structure, the density of this feature is lower than expected for RNA. In contrast, the same feature is strong when ribosomes for cryo-EM are purified without subjecting them to an in vitro translation system (Gomez-Lorenzo et al., 2000). This behavior can be partially explained by a large conformational change occurring at this element, discussed in the accompanying paper (Beckmann et al., 2001).

Two more expansion segments are located at the bottom of the 60S subunit. ES24, an extension of helix 59 of 25S rRNA, appears to be involved in the binding of Sec61 (Beckmann et al., 2001). ES41, an extension of helix 101 of 25S rRNA (Figure 2b), makes an intersubunit bridge with the 40S subunit (Figure 6, see below).

The Protein Distribution in the 60S Subunit

Homology models of 28 yeast LSU proteins were calculated and docked into the cryo-EM map (Supplemental Table S2). Density clusters in the 60S subunit protein map that are not accounted for by homology models predict the positions of the 17 proteins for which the exact position is still unknown, as well as additional domains in the homologous proteins (Figure 4). There are 12 regions with additional protein density at the surface of the 60S subunit, most of which are present at the solvent side.

The large protein cluster building the extended stalk can be identified as the P0/P1/P2 complex, the homolog of the bacterial L10(L7/L12)$_4$ complex. As noted earlier, the extended stalk in yeast has a different orientation compared to the extended stalk in bacteria (Gomez-Lorenzo et al., 2000). Interestingly, the P0/P1/P2 density has a sidelobe that is located close to the N-terminal domain of rpL12 (L11p). Exactly at this location, a contact occurs between the stalk-base region and elongation factor EF2 (Gomez-Lorenzo et al., 2000), a contact that has never been observed in any of the 70S•EF-G complexes from *E. coli* (Frank and Agrawal, 2000). A direct and unique interaction of the P proteins with EF2 would give a structural explanation for their ability to discriminate between EF2 and EF-G (Uchiumi et al., 1999).

Apart from the cluster corresponding to the P proteins, the lack of data about the quaternary structure of eukaryotic ribosomes by IEM, cross-linking, or footprinting experiments does not allow further analysis. An overview of the unidentified protein densities and their neighborhood in the 60S subunit is presented in Supplemental Table S3. The vast majority of these clusters appear to contact more than one component, and the additional ribosomal proteins in yeast might have structural tasks, e.g., stabilizing the tertiary fold of the LSU rRNA, or they might interact with components of the eukaryotic environment.

Intersubunit Bridges between the 40S and the 60S Subunit

Protein synthesis requires communication between the small and the large subunit. For example, signals from

Table 1. Bridges between the 40S and 60S Ribosomal Subunits

		40S		60S	
Bridge	Type	Component	Approximate Position	Component	Approximate Position
B1a	p-R	rpS15 (S19p)		25S h38	889
B1b/c	p-p	rpS18 (S13p)		rpL11 (L5p)	
B2a	R-R	18S h44	1408/1493 min	25S h69	1910-1920 min
B2b	R-R	18S h24	784/800	25S h68	1847
	R-R	18S h45	1515	25S	1939-1941
B2c	R-R	18S h27	899	25S h62	1693
				25S h67	1832
B2d	R-R	18S h23	702	25S h68	1848/1895 min
B2e	R-p	18S h22	671	rpL2 (L2p)	
	R-p	18S h23	713	rpL2 (L2p)	
				rpL43 (L37ae)	
B3	R-R	18S h44	1420/1481 min	25S h71	1948/1960 min
B4	R-R	18S h11	247	25S h34	711/720 min
	R-R	18S h20	583/761 min	25S h34	716 lo
	p-R	rpS13 (S15)		25S h34	716 lo
B5a	R-p	18S h44	1422 bb	rpL23 (L14p)	
B5b	R-R	18S h44	1428/1472 min	25S h62	1689/1704 min
B6	R-p	18S h14	343	rpL23 (L14p)	
B7	R-p	18S h44	1446	rpL24 (L24e)	
eB8	p-R	rpSx		25S h79	Expansion
eB9	p-p	rpSx		RpLx	
	R-p	18S h21	Expansion		
eB10	R-R	18S h11	272	25S h63	1713/1747 min
	p-R	rpSx			
eB11	R-R	18S h9	187	25S h101	Expansion
	p-R	rpSx			

bb, backbone; lo, loop; min, minor groove

the decoding center on the SSU to the peptidyl transferase center on the LSU can be transmitted either by ligands that contact both regions, e.g., bound tRNAs, or by the intersubunit bridges that connect the subunits. The structure of the intersubunit bridges and their dynamics are therefore of particular importance for an understanding of the mechanism of protein synthesis.

Six bridges were observed earlier in low-resolution maps of the *E. coli* 70S ribosome (Frank et al., 1995; Lata et al., 1996). The nomenclature B1–B6 to describe them was further elaborated in the context of the analysis of a 7.8 Å resolution X-ray map of the *T. thermophilus* 70S ribosome (Cate et al., 1999) and a 11.5 Å resolution cryo-EM map of the *E. coli* 70S ribosome (Gabashvili et al., 2000). A first attempt has been made to describe the bridges in a mammalian 80S ribosome at approximately 25 Å resolution (Morgan et al., 2000). The present 15.4 Å resolution cryo-EM map of the *S. cerevisiae* 80S ribosome allows us to describe the intersubunit bridges in eukaryotic ribosome at the level of detail that is comparable to that achieved for the intersubunit bridges in bacterial ribosomes (Figure 6). The docking of X-ray models of the rRNAs and homology models of the ribosomal proteins has allowed us to go even a step further and determine the molecular identity of most of the ribosomal components involved in subunit-subunit interaction, as has been done in the recent 5.5 Å resolution X-ray map of the *T. thermophilus* 70S ribosome (Yusupov et al., 2001).

All the bridges that have been discovered in the bacterial 70S ribosomes have a corresponding bridge in the yeast 80S ribosome. This remarkable evolutionary conservation demonstrates the importance of these bridges. Most of the intersubunit contacts involve RNA-RNA interactions (see also Mitchell et al., 1992; Merryman et al., 1999a, 1999b; Yusupov et al., 2001), although various RNA-protein interactions and one protein-protein contact can be identified (Table 1). Several of the RNA interactions clearly involve minor groove sites. Interestingly, in addition to the conserved set of bridges, four new bridges can be identified in the yeast 80S ribosome that might be specific for eukaryotic ribosomes (Figure 6). We therefore extend the current B1–B7 nomenclature for bacterial ribosomes and name the additional intersubunit contacts eB8–eB11.

Two bridges connect the head of the 40S subunit with the central protuberance of the 60S subunit. The apical loop of helix 38 of 25S rRNA (A site finger) interacts with rpS15 (S19p) to form bridge B1a. The 30S part of B1a in *T. thermophilus* has been identified as S13 and not S19 (Yusupov et al., 2001). Since rpS18 (S13p) appears to have a somehow changed position in yeast compared to *T. thermophilus* and also lacks the C-terminal extension that contacts the P site-bound tRNA, this potential difference might be species-related, although higher resolution of the yeast ribosome will be required to solve this question unequivocally. B1b, the sole bridge that does not involve RNA, is formed by an interaction of rpS18 (S13p) with rpL11 (L5p) (Figure 6 and Table 1).

Most of the bridges that connect the main part of the 60S subunit with the body/platform domains of the 40S subunit are lying approximately on three parallel lines that run from the top to the bottom of the subunits. The bridges on the line closest to the shoulder of the 40S or the stalk region of the 60S subunit are B2a, B3, B5a, B5b, eB10, and eB11 (Figure 6). B2a, B3, and B5b are all formed by minor groove-minor groove interactions between helix 44 of 18S rRNA and helices of domain IV

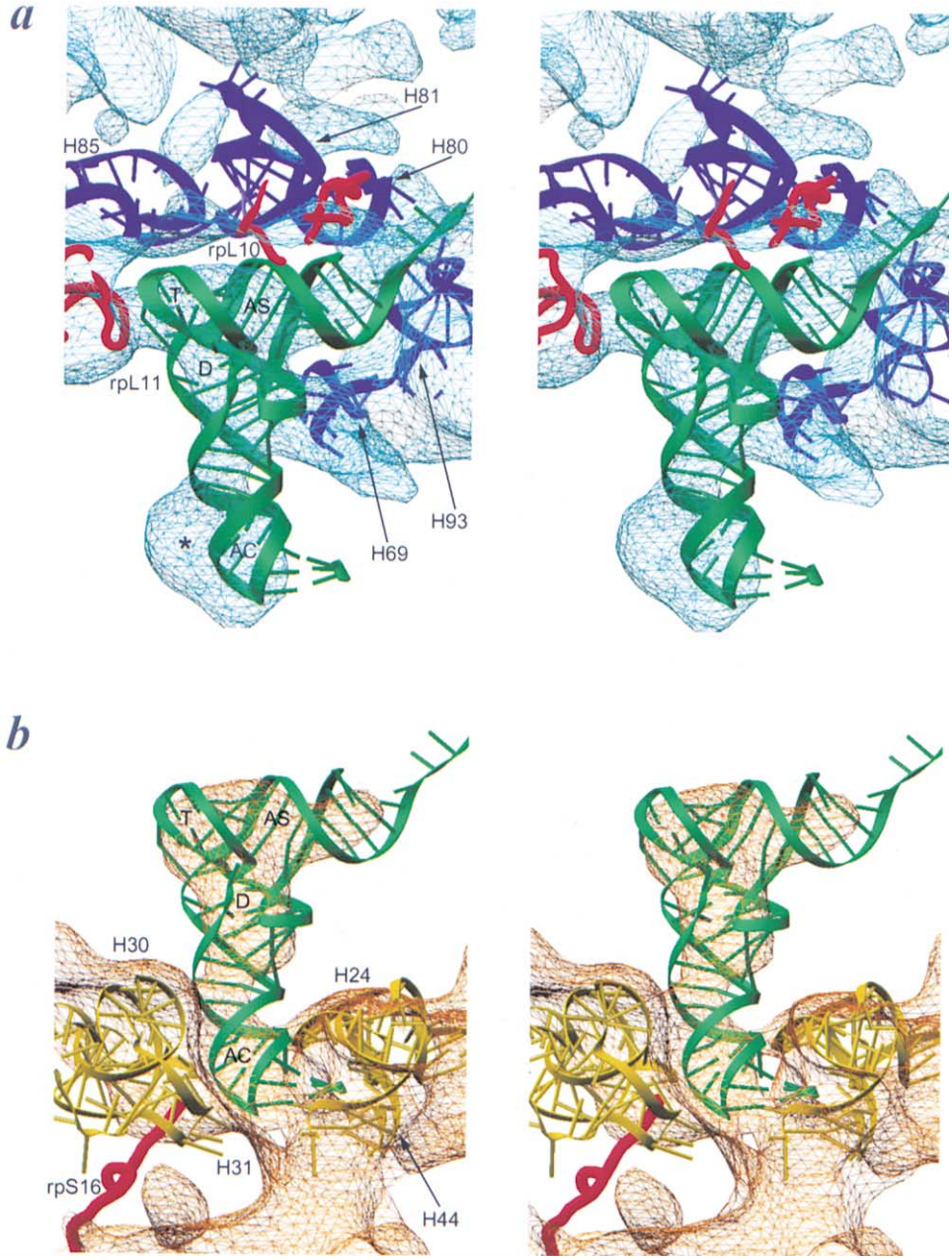

Figure 7. Molecular Environment of the P Site-Bound tRNA in the Yeast 80S Ribosome

Stereo pictures show the tRNA density together with surrounding density of the 60S subunit in blue (a) and 40S subunit in yellow (b). Fitted atomic models, corresponding to the P site-bound tRNA and its molecular environment (Table 2), are shown in the ribbon representation. The ribosomal components are designated, as are the domains of the tRNA: AC, anticodon loop; AS, acceptor stem; D, D loop; T, T loop. The asterix (a) indicates density that belongs to the 40S subunit and is broadly fused to the tRNA density.

of 25S rRNA. B5a is due to an RNA-protein contact between helix 44 of 18S rRNA and rpL23 (L14p). Further down the hypothetical line that connects these bridges are the additional bridges eB10 and eB11, which are among the strongest intersubunit connections in the yeast 80S ribosome. eB10 involves an RNA-RNA contact between 18S rRNA helix 11 and 25S rRNA helix 63. The participation of an unknown eukaryote-specific protein in this bridge might explain why it is not formed in bacterial ribosomes. eB11 is formed by an RNA-RNA interaction between 18S rRNA helix 9 and the expansion of helix 101 of 25S rRNA. This bridge also involves an unknown protein of the 40S subunit.

Helix 44 of 16S rRNA is bent toward the shoulder side of the 40S subunit to become the "left foot" at its apical domain. The kink is approximately at the position of the bridge B5b (Figure 6). Further down, B7 is yet another bridge that involves helix 44 of 18S rRNA. Its partner on the 60S subunit is rpL24 (L24e). B7 has been previously observed in the *T. thermophilus* 70S ribosome, where

Table 2. Contacts between the P Site Bound Peptidyl-tRNA and the 80S Ribosome from Yeast

Ribosomal Subunit	Approximate tRNA Position	Ribosomal Component	Approximate Ribosome Position
40S	29/30	18S h30	1229/1230
	32	rpS16 (S9p)	Tyr141/Arg142
	34	18S h31	966
	39	18S h24	790
	41/42	18S h43	1338/1339
	mRNA codon	18S h44	1400/1402
60S	2	rpL10 (L10e)	Lys101
	3/4	25S h80	2285/2286
	11-13	25S h69	1908-1910
	14	25S h69	1924
	51/52/63	rpL10 (L10e)	Arg24
	56	rpL11 (L5p)	Tyr51
	71/72	25S h93	2594
	73	25S h93	2602

it has been named B6 (Cate et al., 1999). rpL24 has no homologous protein in bacteria, and therefore, this bridge is formed by an analogous protein in *T. thermophilus*. Indeed, this contact has been attributed to protein L19p in the X-ray structure of the *T. thermophilus* 70S ribosome at improved resolution (Yusupov et al., 2001).

Bridges B2b, B2c, and B4 are lying on the second and central line (Figure 6). B2b and B2c are formed by RNA-RNA interactions that again involve domain IV of 25S rRNA. B2b involves helix 24 of 18S rRNA and the last helix at the 3′ end, helix 45. B2c encompasses helix 27, the switch helix of 18S rRNA. B4 has been previously identified in *T. thermophilus* as an RNA-protein contact between S15 and helix 34 of 23S rRNA (Culver et al., 1999). In yeast, this bridge is also formed by helix 34 of 25S rRNA and rpS13 (S15p), but it appears to involve additional RNA-RNA contacts between helix 34 of 25S rRNA and helices 11 and 10 of 18S rRNA (Table I).

The third line of bridges on the L1 side of the 60S subunit comprises B2d, B2e, and eB9 (Figure 6). B2d is a contact between helix 23 of 18S rRNA in the platform of the 40S subunit and the minor groove of helix 68 of domain IV of 25S rRNA. B2e was first observed in the *E. coli* 70S ribosome (Gabashvili et al., 2000) and was named B8 in the *T. thermophilus* 70S ribosome (Yusupov et al., 2001). B2e is an RNA-protein contact that involves rpL8 (L2p). The presence of protein L2 in *E. coli* has been shown to be crucial for the ability of the 50S subunit to associate with the 30S subunit (Diedrich et al., 2000). In yeast, rpL43 (L37ae) also appears to be involved in this connection, and the 40S counterparts are helices 22 and 23 of 18S rRNA. eB9 is built by components that are not present in bacterial ribosomes (Figure 6). It appears to make use of a protein-protein contact between unknown proteins, or an RNA-protein contact between an unknown LSU protein and the helix 21 insertion in 18S rRNA.

Two more bridges are present at the outside of the intersubunit face of the subunits (Figure 6). B6 is formed by a contact between 18S rRNA helix 14 and protein rpL23 (L14p). eB8, located below the L1 protuberance, is formed by an unknown 40S protein and ES31, an insertion into helix 79 of 25S rRNA (see also Figure 5). Since helix 79 is stacked onto the L1-bearing helix 76, bridge eB8 could be important in controlling the large conformational change that affects the position of the L1 protuberance in the yeast 80S ribosome.

tRNA-Ribosome Interaction at the P Site

During protein synthesis, a tRNA has to interact with the ribosome in at least two regions. The anticodon loop of the tRNA and the mRNA codon have to interact with the ribosomal decoding center on the SSU. The 3′-CCA end of the tRNA has to contact the peptidyltransferase center located on the LSU. tRNA-ribosome interactions in these two regions are well documented for bacterial ribosomes by various biochemical techniques, e.g., footprinting, cross-linking and genetic studies (for review see Green and Noller, 1997; Brimacombe, 1995) and have been directly observed by cryo-EM (Stark et al., 1997a; Agrawal et al., 2000; Gabashvili et al., 2000) and X-ray crystallography (Cate et al., 1999; Yusupov et al., 2001; Nissen et al., 2000; Carter et al., 2000). In addition, tRNA-ribosome interactions at the elbow region of the tRNA have been suggested by phosphorothioate footprints that occur in the T loop and D loop of the tRNA upon ribosome binding (Dabrowski et al., 1995). Indeed, contacts between the tRNA and the ribosome at the tRNA elbow have been visualized by cryo-EM in various functional complexes of the *E. coli* 70S ribosome (Agrawal et al., 2000; Gabashvili et al., 2000; Malhotra et al., 1998). However, no information is available yet on the structural basis of the tRNA-ribosome interaction in eukaryotic cells.

The 15.4 Å resolution cryo-EM map of the translating 80S ribosome from yeast clearly displays an L-shaped density in the intersubunit space that corresponds to the P site-bound peptidyl-tRNA in its entirety (Figure 7). Only the single-stranded 3′-CCA end is not resolved. The density shows indications of major and minor grooves of the tRNA molecule and allows an accurate docking of the atomic structure of the tRNA into the density map. The X-ray structure of the isolated $tRNA^{Phe}$ from yeast (Hingerty et al., 1978) and the structure of the tRNA derived from a tRNA•70S complex from *T. thermophilus* (Cate et al., 1999; Yusupov et al., 2001) were used for the docking. The latter tRNA model has a somewhat changed conformation when compared to the isolated tRNA, implying a conformational change of the tRNA upon binding to the ribosomal P site. This tRNA model appears to fit better into the yeast cryo-

EM map. The conformational change of the tRNA that is implicit in the structure of the 70S-bound *T. thermophilus* tRNA (Cate et al., 1999; Yusupov et al., 2001) might therefore also occur in yeast. Moreover, a conformational change of the tRNA upon binding to the ribosome has been suggested by phosphorothiate footprinting experiments (Dabrowski et al., 1995).

The tRNA density is fused with the ribosome density at several discrete positions. These apparent contacts involve all four domains of the tRNA (Figure 7). The docking of models for the rRNAs, the ribosomal proteins, and the tRNA allows the parts of the molecules involved in these contacts to be determined, and thereby strong candidates for actual molecular interactions to be identified (Table 2). Only a smaller part of the tRNA interacts with the 40S subunit of yeast (see also Nierhaus et al., 2000). The anticodon stem-loop is positioned between the head and body/platform of the 40S subunit (Figure 1e). On the body/platform side, the P site codon appears to interact with the top of helix 44 of 18S rRNA and tRNA with the apical loop of helix 24 in the platform. From the opposite side, the tRNA is clamped down by 40S components belonging to the head. Helices 30, 31, and 43 of 18S rRNA, as well as an extended part of rpS16 (S9p), are likely to be involved in these interactions (Figure 7 and Table 2), which in yeast appear to be very similar to those described for a bacterial system (Carter et al., 2000; Yusupov et al., 2001).

A second protein-tRNA contact has been described for *T. thermophilus* (Carter et al., 2000; Yusupov et al., 2001). However, the long tail of S13 that interacts with the tRNA in *T. thermophilus* does not have a corresponding sequence for rpS18. Moreover, rpS18 (S13p) in yeast appears to have a somewhat changed position compared to the position of S13 in the *T. thermophilus* 30S subunit. Therefore, the tRNA contact with the S9p protein family is evolutionary conserved, in contrast to the tRNA contact with the S13p protein family.

Three of the four tRNA domains interact with the large ribosomal subunit (Table 2). The D loop makes a contact with helix 69 of 25S rRNA and the T loop interacts with rpL11 (L5p). The same interactions have been proposed for the *E. coli* ribosome (Spahn et al., 2000) and the *T. thermophilus* ribosome (Yusupov et al., 2001). Interestingly, both components of the LSU are involved in the formation of bridges with the SSU, a fact which might have implications for the dynamics of translation, i.e., specifically the mechanism of translocation. The 3′-CCA end of the tRNA is not resolved in the yeast cryo-EM map, but the end of the tRNA acceptor stem appears to contact the 60S subunit. This interaction might involve helices 80 (the apical loop of helix 80 participates in a base-pairing interaction with the 3′-CCA end of the tRNA [Samaha et al., 1995; Nissen et al., 2000]) and 93 of 25S rRNA, as well as protein rpL10 (L10e). At a lower density threshold (not shown), an additonal contact can be observed that involves the TΨC stem of the tRNA and protein rpL10 (L10e). We note that in *T. thermophilus*, no interaction between the P site-bound tRNA and L16p (Yusupov et al., 2001), which occupies the same position as rpL10 (L10e) in yeast, has been reported, and it remains to be seen if this weaker contact reflects an actual interaction.

Conclusions

We have presented here an interpretation of a cryo-EM map of an eukaryotic 80S ribosome in terms of atomic RNA and protein models. The common core of the eukaryotic ribosome agrees very well with X-ray structures of the bacterial and archaebacterial subunits and reinforces the notion that the fundamental mechanism of protein synthesis is highly conserved throughout all kingdoms. This view is supported by the finding that the intersubunit bridges and the ribosome-tRNA interactions are highly conserved, as well. Nevertheless, a few unexpected differences exist even in this highly conserved region. The most pronounced differences in appearance between eukaryotic and bacterial ribosomes are due to expansion segments in the rRNAs and additional proteins that are present mainly at the surface of the solvent sides of the 40S and 60S subunits. Even though these elements are far away from the primary functional centers, the additional tertiary and quaternary interactions could be important for ribosome dynamics, as also suggested by the emergence of four new intersubunit bridges. Moreover, the additional components are likely to interact with other cellular components, outside of the immediate process of protein synthesis. Our model of the yeast 80S ribosome provides the basis for molecular-level interpretations of the interactions of the eukaryotic ribosomes within the context of the eukaryotic environment.

Experimental Procedures

The cryo-EM map of the 80S ribosome (Beckmann et al., 2001) was computationally separated into rRNA and protein maps using a recently developed method that takes into account the differences in the density distribution of RNA and proteins, as well as the molecular masses and contiguity constraints (Spahn et al., 2000).

Homology models for the yeast ribosomal proteins were constructed using the large-scale protein structure modeling pipeline as implemented in ModPipe (Sanchez and Sali, 1998) and deposited into a relational database for homology models, ModBase ((Sanchez et al., 2000); http://guitar.rockefeller.edu/modbase). Structural templates used to calculate the models consisted of all the individual chains from structures in PDB (as of September 2000), clustered such that the sequences of no two chains from any two clusters were more than 95% identical. In addition, the structures of the small subunit from *T. thermophilus* (PDB code: 1FJF) and the large subunit from *H. morismortui* (PDB code: 1FKF) were considered as separate sets of templates.

Sequence structure matches were established by aligning the psi-blast generated profile (Altschul et al., 1997) of the yeast sequences against each of the template sequences and also by scanning the yeast sequences against a database of psi-blast generated profiles of the template sequences using IMPALA (Schaffer et al., 1999). Significant alignments covering distinct regions of the yeast sequences were chosen for modeling. Models were calculated for each one of the sequence-structure matches using MODELLER (Sali and Blundell, 1993). The resulting models were then evaluated using a scheme based on statistical potentials that uses the compactness of the model, the sequence identity of the sequence-structure match, and energy z-scores to the assess the quality of the model.

Models for docking into the EM-map were selected based on the e-value of the alignment, the quality of the final model, and the template structure on which they were based. The selected models represent alignments with sequence identities in the range 20%–56% (with an average of 32%) and e-values better than 10^{-4}. The coverage of the models (fraction of the yeast ribosomal sequence modeled) ranges between 34%–99% (with an average of 75%).

Docking of atomic models into the cryo-EM density map was done manually using O (Jones et al., 1991). The figures were pre-

pared using IRIS Explorer (Numerical Algorithms Group, Inc., Downers Grove, IL), POV-Ray, and Ribbons (Carson, 1991).

Acknowledgments

We are grateful to Michael Watters and Jan Giesebrecht for assistance with the illustrations and to Dr. Ursula Pieper for her help with ModBase. A.S. is an Irma T. Hirschl Trust Career Scientist. This work was supported by a grant of the Volkswagen Stiftung (to R.B.), a Merck Genome Research Award (to A.S.), and grants from NIH (GM 54762 to A.S., R37 GM29169 and P41 RR01219 to J.F., and R01 GM60635 to P.A.P.) and NSF (BIR 9219043 to J.F.).

Received August 8, 2001; revised September 21, 2001.

References

Agrawal, R.K., and Frank, J. (1999). Structural studies of the translational apparatus. Curr. Opin. Struct. Biol. *9*, 215–221.

Agrawal, R.K., Spahn, C.M.T., Penczek, P., Grassucci, R.A., Nierhaus, K.H., and Frank, J. (2000). Visualization of tRNA movements on the *Escherichia coli* 70S ribosome during the elongation cycle. J. Cell Biol. *150*, 447–459.

Altschul, S.F., Madden, T.L., Schaffer, A.A., Zhang, J., Zhang, Z., Miller, W., and Lipman, D.J. (1997). Gapped BLAST and PSI-BLAST: a new generation of protein database search programs. Nucleic Acids Res. *25*, 3389–3402.

Ban, N., Nissen, P., Hansen, J., Moore, P.B., and Steitz, T.A. (2000). The complete atomic structure of the large ribosomal subunit at 2.4 Å resolution. Science *289*, 905–920.

Beckmann, R., Bubeck, D., Grassucci, R., Penczek, P., Verschoor, A., Blobel, G., and Frank, J. (1997). Alignment of conduits for the nascent polypeptide chain in the ribosome-Sec61 complex. Science *278*, 2123–2126.

Beckmann, R., Spahn, C.M.T., Eswar, N., Helmers, J., Penczek, P.A., Sali, A., Frank, J., and Blobel, G. (2001). Architecture of the protein-conducting channel associated with the translating 80S ribosome. Cell *107*, this issue, 361–372.

Brimacombe, R. (1995). The structure of ribosomal RNA: a three-dimensional jigsaw puzzle. Eur. J. Biochem. *230*, 365–383.

Carson, M. (1991). Ribbons 2.0. J. Appl. Cryst. *24*, 103–106.

Carter, A.P., Clemons, W.M., Jr., Brodersen, D.E., Morgan-Warren, R.J., Wimberly, B.T., and Ramakrishnan, V. (2000). Functional insights from the structure of the 30S ribosomal subunit and its interactions with antibiotics. Nature *407*, 340–348.

Carter, A.P., Clemons, W.M., Jr., Brodersen, D.E., Morgan-Warren, R.J., Hartsch, T., Wimberly, B.T., and Ramakrishnan, V. (2001). Crystal structure of an initiation factor bound to the 30S ribosomal subunit. Science *291*, 498–501.

Cate, J.H., Yusupov, M.M., Yusupova, G.Z., Earnest, T.N., and Noller, H.F. (1999). X-ray crystal structures of 70S ribosome functional complexes. Science *285*, 2095–2104.

Culver, G.M., Cate, J.H., Yusupova, G.Z., Yusupov, M.M., and Noller, H.F. (1999). Identification of an RNA-protein bridge spanning the ribosomal subunit interface. Science *285*, 2133–2135.

Dabrowski, M., Spahn, C.M., and Nierhaus, K.H. (1995). Interaction of tRNAs with the ribosome at the A and P sites. EMBO J. *14*, 4872–4882.

Diedrich, G., Spahn, C.M.T., Stelzl, U., Schafer, M.A., Wooten, T., Bochariov, D.E., Cooperman, B.S., Traut, R.R., and Nierhaus, K.H. (2000). Ribosomal protein L2 is involved in the association of the ribosomal subunits, tRNA binding to A and P sites and peptidyl transfer. EMBO J. *19*, 5241–5250.

Dube, P., Bacher, G., Stark, H., Müller, F., Zemlin, F., van Heel, M., and Brimacombe, R. (1998). Correlation of the expansion segments in mammalian rRNA with the fine structure of the 80 S ribosome; a cryoelectron microscopic reconstruction of the rabbit reticulocyte ribosome at 21 Å resolution. J. Mol. Biol. *279*, 403–421.

Frank, J., and Agrawal, R.K. (2000). A ratchet-like inter-subunit reorganization of the ribosome during translocation. Nature *406*, 318–322.

Frank, J., Zhu, J., Penczek, P., Li, Y., Srivastava, S., Verschoor, A., Radermacher, M., Grassucci, R., Lata, R.K., and Agrawal, R.K. (1995). A model of protein synthesis based on cryo-electron microscopy of the *E. coli* ribosome. Nature *376*, 441–444.

Gabashvili, I.S., Agrawal, R.K., Spahn, C.M.T., Grassucci, R.A., Frank, J., and Penczek, P. (2000). Solution structure of the *E. coli* 70S ribosome at 11.5 Å resolution. Cell *100*, 537–549.

Gerbi, S.A. (1996). Expansion segment: regions of variable size that interrupt the universal core secondary structure of ribosomal RNA. In Ribosomal RNA: Structure, Evolution, Processing, and Function in Protein Synthesis. R.A. Zimmermann and A.E. Dahlberg, eds. (New York: CRC Press), pp. 71–87.

Gomez-Lorenzo, M.G., Spahn, C.M.T., Agrawal, R.K., Grassucci, R.A., Penczek, P., Chakraburtty, K., Ballesta, J.P.G., Lavandera, J.L., Garcia-Bustos, J.F., and Frank, J. (2000). Three-dimensional cryo-electron microscopy localization of EF2 in the *Saccharomyces cerevisiae* 80S ribosome at 17.5 Å resolution. EMBO J. *19*, 2710–2718.

Green, R., and Noller, H.F. (1997). Ribosomes and translation. Annu. Rev. Biochem. *66*, 679–716.

Gutell, R.R., Subashchandran, S., Schnare, M., Du, Y., Lin, N., Madabusi, L., Müller, K., Pande, N., Shang, Z., Date, S., et al. (2001). Comparative Sequence Analysis and the Prediction of RNA Structure (http://www.rna.icmb.utexas.edu).

Hardesty, B., Kramer, G., Tsalkova, T., Ramachandiran, V., McIntosh, B., and Brod, D. (2000). Folding of nascent peptides on ribosomes. In The Ribosome: Structure, Function, Antibiotics, and Cellular Interactions, R.A. Garrett, S.R. Douthwaite, A. Liljas, A.T. Matheson, P.B. Moore, and H.F. Noller, eds. (Washington, D.C.: ASM Press), pp. 287–300.

Hingerty, B., Brown, R.S., and Jack, A. (1978). Further refinement of the structure of yeast $tRNA^{Phe}$. J. Mol. Biol. *124*, 523–534.

Ho, J.H., Kallstrom, G., and Johnson, A.W. (2000). Nmd3p is a Crm1p-dependent adapter protein for nuclear export of the large ribosomal subunit. J. Cell Biol. *151*, 1057–1066.

Jones, T.A., Zhou, J.Y., Cowan, S.W., and Kjeldgaard, M. (1991). Improved methods for building protein models in electron density maps and the location of errors in these models. Acta Crystallogr. A *A47*, 110–119.

Lata, K.R., Agrawal, R.K., Penczek, P., Grassucci, R., Zhu, J., and Frank, J. (1996). Three-dimensional reconstruction of the *Escherichia coli* 30 S ribosomal subunit in ice. J. Mol. Biol. *262*, 43–52.

Malhotra, A., Penczek, P., Agrawal, R.K., Gabashvili, I.S., Grassucci, R.A., Jünemann, R., Burkhardt, N., Nierhaus, K.H., and Frank, J. (1998). *Escherichia coli* 70 S ribosome at 15 Å resolution by cryo-electron microscopy: localization of fMet-$tRNA_f^{Met}$ and fitting of L1 protein. J. Mol. Biol. *280*, 103–116.

Menetret, J., Neuhof, A., Morgan, D.G., Plath, K., Radermacher, M., Rapaport, T.A., and Akey, C.W. (2001). The structure of ribosome-channel complexes engaged in protein translocation. Mol. Cell *6*, 1219–1232.

Merryman, C., Moazed, D., Daubresse, G., and Noller, H.F. (1999a). Nucleotides in 23S rRNA protected by the association of 30S and 50S ribosomal subunits. J. Mol. Biol. *285*, 107–113.

Merryman, C., Moazed, D., McWhirter, J., and Noller, H.F. (1999b). Nucleotides in 16S rRNA protected by the association of 30S and 50S ribosomal subunits. J. Mol. Biol. *285*, 97–105.

Mitchell, P., Osswald, M., and Brimacombe, R. (1992). Identification of intermolecular RNA cross-links at the subunit interface of the *Escherichia coli* ribosome. Biochemistry *31*, 3004–3011.

Morgan, D.G., Ménétret, J.F., Radermacher, M., Neuhof, A., Akey, I.V., Rapoport, T.A., and Akey, C.W. (2000). A comparison of the yeast and rabbit 80S ribosome reveals the topology of the nascent chain exit tunnel, inter-subunit bridges and mammalian rRNA expansion segments. J. Mol. Biol. *301*, 301–321.

Nierhaus, K.H., Spahn, C., Burkhardt, N., Dabrowski, M., Diedrich, G., Einfeldt, E., Kamp, D., Marquez, V., Patzke, S., Schafer, M.A., et al. (2000). Ribosomal elongation cycle. In The Ribosome: Structure,

Function, Antibiotics, and Cellular Interactions. R.A. Garrett, S.R. Douthwaite, A. Liljas, A.T. Matheson, P.B. Moore, and H.F. Noller, eds. (Washington, D.C.: ASM Press), pp. 319–336.

Nissen, P., Hansen, J., Ban, N., Moore, P.B., and Steitz, T.A. (2000). The structural basis of ribosome activity in peptide bond synthesis. Science *289*, 920–930.

Noller, H.F. (1991). Ribosomal RNA and translation. Annu. Rev. Biochem. *60*, 191–227.

Ogle, J.M., Brodersen, D.E., Clemons, W.M., Jr., Tarry, M.J., Carter, A.P., and Ramakrishnan, V. (2001). Recognition of cognate transfer RNA by the 30S ribosomal subunit. Science *292*, 897–902.

Pioletti, M., Schlünzen, F., Harms, J., Zarivach, R., Gluhmann, M., Avila, H., Bashan, A., Bartels, H., Auerbach, T., Jacobi, C., et al. (2001). Crystal structures of complexes of the small ribosomal subunit with tetracycline, edeine and IF3. EMBO J. *20*, 1829–1839.

Planta, R.J., and Mager, W.H. (1998). The list of cytoplasmic ribosomal proteins of *Saccharomyces cerevisiae*. Yeast *14*, 471–477.

Rossmann, M.G. (2000). Fitting atomic models into electron-microscopy maps. Acta Crystallogr. D *D56*, 1341–1349.

Sachs, A.B., Sarnow, P., and Hentze, M.W. (1997). Starting at the beginning, middle, and end: translation initiation in eukaryotes. Cell *89*, 831–838.

Sali, A., and Blundell, T.L. (1993). Comparative protein modelling by satisfaction of spatial restraints. J. Mol. Biol. *234*, 779–815.

Samaha, R.R., Green, R., and Noller, H.F. (1995). A base pair between tRNA and 23S rRNA in the peptidyl transferase centre of the ribosome. Nature *377*, 309–314.

Sanchez, R., and Sali, A. (1998). Large-scale protein structure modeling of the *Saccharomyces cerevisiae* genome. Proc. Natl. Acad. Sci. USA *95*, 13597–13602.

Sanchez, R., Pieper, U., Mirkovic, N., de Bakker, P.I., Wittenstein, E., and Sali, A. (2000). MODBASE, a database of annotated comparative protein structure models. Nucleic Acids Res. *28*, 250–253.

Schaffer, A.A., Wolf, Y.I., Ponting, C.P., Koonin, E.V., Aravind, L., and Altschul, S.F. (1999). IMPALA: matching a protein sequence against a collection of PSI-BLAST-constructed position-specific score matrices. Bioinformatics *15*, 1000–1011.

Schlünzen, F., Tocilj, A., Zarivach, R., Harms, J., Glühmann, M., Janell, D., Bashan, A., Bartels, H., Agmon, I., Franceschi, F., and Yonath, A. (2000). Structure of functionally activated small ribosomal subunit at 3.3 Å resolution. Cell *102*, 615–623.

Spahn, C.M.T., and Prescott, C.D. (1996). Throwing a spanner in the works: antibiotics and the translation apparatus. J. Mol. Med. *74*, 423–429.

Spahn, C.M.T., Grassucci, R.A., Penczek, P., and Frank, J. (1999). Direct three-dimensional localization and positive identification of RNA helices within the ribosome by means of genetic tagging and cryo-electron microscopy. Structure *7*, 1567–1573.

Spahn, C.M.T., Penczek, P., Leith, A., and Frank, J. (2000). A method for differentiating proteins from nucleic acids in intermediate-resolution density maps: cryo-electron microscopy defines the quaternary structure of the *Escherichia coli* 70S ribosome. Structure Fold. Des. *8*, 937–948.

Spahn, C.M.T., Kieft, J.S., Grassucci, R.A., Penczek, P., Zhou, K., Doudna, J.A., and Frank, J. (2001). Hepatitis C virus IRES RNA-induced changes in the conformation of the 40S ribosomal subunit. Science *291*, 1959–1962.

Stark, H., Orlova, E.V., Rinke-Appel, J., Junke, N., Müller, F., Rodnina, M., Wintermeyer, W., Brimacombe, R., and van Heel, M. (1997a). Arrangement of tRNAs in pre- and posttranslocational ribosomes revealed by electron cryomicroscopy. Cell *88*, 19–28.

Stark, H., Rodnina, M.V., Rinke-Appel, J., Brimacombe, R., Wintermeyer, W., and van Heel, M. (1997b). Visualization of elongation factor Tu on the *Escherichia coli* ribosome. Nature *389*, 403–406.

Stark, H., Rodnina, M.V., Wieden, H.J., van Heel, M., and Wintermeyer, W. (2000). Large-scale movement of elongation factor G and extensive conformational change of the ribosome during translocation. Cell *100*, 301–309.

Triana-Alonso, F.J., Chakraburtty, K., and Nierhaus, K.H. (1995). The elongation factor 3 unique in higher fungi and essential for protein biosynthesis is an E site factor. J. Biol. Chem. *270*, 20473–20478.

Uchiumi, T., Hori, K., Nomura, T., and Hachimori, A. (1999). Replacement of L7/L12.L10 protein complex in *Escherichia coli* ribosomes with the eukaryotic counterpart changes the specificity of elongation factor binding. J. Biol. Chem. *274*, 27578–27582.

Verschoor, A., Warner, J.R., Srivastava, S., Grassucci, R.A., and Frank, J. (1998). Three-dimensional structure of the yeast ribosome. Nucleic Acids Res. *26*, 655–661.

Wimberly, B.T., Guymon, R., McCutcheon, J.P., White, S.W., and Ramakrishnan, V.R. (1999). A detailed view of a ribosomal active site: The structure of the L11-RNA complex. Cell *97*, 491–502.

Wimberly, B.T., Brodersen, D.E., Clemons, W.M., Jr., Morgan-Warren, R.J., Carter, A.P., von Rhein, C., Hartsch, T., and Ramakrishnan, V. (2000). Structure of the 30S ribosomal subunit. Nature *407*, 327–339.

Wittmann-Liebold, B. (1986). Ribosomal proteins: their structure and evolution. In Structure, Function, and Genetics of Ribosomes, B. Hardesty and G. Kramer, eds. (New York: Springer-Verlag), pp. 326–361.

Wool, I.G., Endo, Y., Chan, Y.L., and Glück, A. (1990). Structure, function, and evolution of mammalian ribosomes. In The Ribosome: Structure, Function, & Evolution. W.E. Hill, A.E. Dahlberg, R.A. Garrett, P.B. Moore, D. Schlessinger, and J.R.Warner, eds. (Washington, D.C.: ASM Press), pp. 203–214.

Yusupov, M.M., Yusupova, G.Z., Baucom, A., Lieberman, K., Earnest, T.N., Cate, J.H., and Noller, H.F. (2001). Crystal structure of the ribosome at 5.5 Å resolution. Science *292*, 883–896.

Accession Numbers

The atomic coordinates of the modeled yeast 80S structure have been deposited in the RCSB Protein Data Bank with accession codes 1K5X, 1K5Y, and 1K5Z.